Journal of Inflammation Research

Dovepress
Taylor & Francis Group

Open Access Full Text Article

ORIGINAL RESEARCH

Exploring the Mechanism of Action of Xuebijing Injection in Treating Acute Respiratory Distress Syndrome Based on Network Pharmacology and Animal Experiments

Jin Li[1,*], Meirong Shen[2,*], Zuan Yin[3]

[1]Department of Intensive Care Unit, The Affiliated Hospital of Jiangxi University of Chinese Medicine, Nanchang City, Jiangxi Province, 330006, People's Republic of China; [2]Department of Intensive Care Unit, Ganzhou People's Hospital, Ganzhou City, Jiangxi Province, 341000, People's Republic of China; [3]Department of Emergency, Jiangxi Provincial People's Hospital, The First Affiliated Hospital of Nanchang Medical College, Nanchang City, Jiangxi Province, 330006, People's Republic of China

*These authors contributed equally to this work

Correspondence: Zuan Yin, Department of Emergency, Jiangxi Provincial People's Hospital, 152 Aiguo Road, Donghu District, Nanchang City, Jiangxi Province, 330006, People's Republic of China, Email yuzan201709@126.com

Objective: To explore the mechanism of Xuebijing injection (XBJ) in treating acute respiratory distress syndrome (ARDS) using network pharmacology and animal experiments.

Methods: Active ingredients of XBJ were analyzed via TCMSP, and ARDS-related targets were identified through DisGENET and Genecard. Intersection targets were obtained using PubChem and Venn diagrams. Protein interaction networks, GO, and KEGG enrichment analyses were conducted. An ARDS rat model was established using lipopolysaccharide (LPS), and rats were divided into control, LPS, and XBJ-treated groups (low, medium, high doses, n=10). Lung wet/dry (W/D) ratio, inflammatory cytokines (IL-17, IL-6, IL-1β, TNF-α), MPO levels, lung pathology, and protein expression of ICAM-1 and HIF-1α were assessed via ELISA, HE staining, immunohistochemistry, and Western blot.

Results: A total of 204 ARDS targets were identified, with 46 intersection targets, mainly TNF-α, MPO, HIF-1α, and ICAM-1. XBJ affected ARDS through IL-17, HIF-1, and TNF signaling pathways. In vivo, LPS-induced lung injury showed alveolar destruction, edema, and inflammation, with increased W/D ratio, cytokines, MPO, and protein expression of HIF-1α and ICAM-1 ($P<0.05$). XBJ treatment alleviated lung damage, reduced inflammation, and improved pathology in a dose-dependent manner ($P<0.05$).

Conclusion: XBJ alleviates ARDS by regulating immune function, oxidative stress, and inflammation through IL-17, HIF-1, and TNF pathways.

Keywords: network pharmacology, Xuebijing injection, acute respiratory distress syndrome, lipopolysaccharide

Introduction

Acute respiratory distress syndrome (ARDS) is caused by direct or indirect acute lung injury leading to alveolar edema, with a severe inflammatory response that can result in respiratory failure. The mortality rate of ARDS is gradually increasing, drawing more and more attention.[1,2] However, there is currently a lack of effective treatment methods for ARDS, especially since single drugs often fail to achieve ideal clinical outcomes.[3] Xuebijing injection (XBJ), a traditional Chinese medicine derivative composed of Paeoniae Radix Rubra, Chuanxiong Rhizoma, Salviae Miltiorrhizae Radix et Rhizoma, Carthami Flos, and Angelicae Sinensis Radix, contains various active ingredients and has been used to treat severe lung infections induced by sepsis, systemic inflammatory response syndrome, and ARDS. Nevertheless, its mechanism of action remains to be studied.[4] Traditional Chinese medicine formulations contain multiple components, targets, and pathways, which cannot be elucidated using conventional methods. Network pharmacology, based on the analysis of big data and systems biology, helps

Received: 17 December 2024
Accepted: 26 April 2025
Published: 7 May 2025

understand the relationships between diseases, targets, and drugs.[5] This study aims to explore the multi-component, multi-target, and multi-pathway therapeutic mechanisms of XBJ in the treatment of ARDS using a network pharmacology approach. An in vivo ARDS rat model was established using lipopolysaccharide (LPS), a major component of the cell wall of Gram-negative bacteria. LPS activates the innate immune system, triggering an excessive inflammatory response that leads to bronchoconstriction, increased pulmonary vascular resistance, and airway hyperresponsiveness, ultimately resulting in ARDS.[6] Intervention with XBJ in ARDS rats lays a foundation for its therapeutic application in ARDS.

Materials and Methods

Materials

Collection of Active Ingredients in XBJ

Using the TCMSP database, the main traditional Chinese medicines in XBJ, "Carthami Flos", "Paeoniae Radix Rubra", "Angelicae Sinensis Radix", "Salviae Miltiorrhizae Radix et Rhizoma", and "Chuanxiong Rhizoma" were sequentially searched. The retrieved active ingredients were screened with the criteria: oral bioavailability (OB) >30% and drug-likeness >0.18.

Collection of ARDS Disease Targets

Using the DisGENET and Genecard databases, the disease targets were searched with the English term "acute respiratory distress syndrome" for ARDS.

Intersection of Active Targets in XBJ and ARDS Targets

The three-dimensional structures of active ingredients in XBJ were collected through the PubChem database and imported into the SwissTargetPrediction database to predict the potential targets of XBJ active ingredients. The deduplicated targets and ARDS targets were then input into the Venny2.1 online data processing platform to obtain the intersection targets of XBJ and ARDS and the Venn diagram.

Construction of Protein-Protein Interaction Network

The intersection targets were imported into the STRING online data analysis platform, selecting "Homo sapiens" for analysis, to obtain the interconnections of intersection target proteins. The obtained protein interaction information was imported into Cytoscape software in ".tsv" format for cluster analysis, yielding the degree (degree) diagram of intersection targets. Targets with a degree ≥30 were selected as core targets.

Gene Ontology (GO) and Kyoto Encyclopedia of Genes and Genomes (KEGG) Enrichment Analysis

GO and KEGG enrichment analysis of these core targets were performed using the DAVID database, selecting "Homo sapiens" as the species. The results were exported and visualized using the online processing software "MicroBix Visualization" for the data with top count values.

Experimental Animals

7-week-old male SD rats, 200–230 g, were purchased from Shandong HuaTewell Biological Technology Co., Ltd. Dongguan Branch, production license number: SCXK (Ji) 2024–007. The animals were acclimated at 24°C-26°C and kept in a 12 h dark and 12 h light cycle, with free access to standard food and water. The experimental protocol was reviewed and approved by the Institutional Animal Ethics Committee, and all operations were conducted according to the guidelines of the Animal Experiment Committee.

Experimental Reagents and Instruments

Carthami Flos, Paeoniae Radix Rubra, Chuanxiong Rhizoma, Salviae Miltiorrhizae Radix et Rhizoma, and Angelicae Sinensis Radix were provided by Tianjin Hongri Pharmaceutical Co., Ltd.; IL-1β, IL-17, IL-6, and TNF-α assay kits were provided by Shanghai Enzyme-linked Biotechnology Co., Ltd.; MPO assay kits, ICAM-1, and HIF-1α primary antibodies were provided by Abcam.

Bio-Rad provided the Model 680 microplate reader; Nikon provided the Eclipse 80i optical microscope.

Methods

Preparation and Intervention of ARDS Rat Model

The ARDS rat model was established by injecting lipopolysaccharide (LPS).[7] A total of 42 rats were randomly selected to establish the ARDS model by intratracheal instillation of 5 mg/kg LPS, while the remaining 12 rats received an equal volume of saline via intratracheal instillation, serving as the control group. Twelve hours after modeling, the ARDS model rats exhibited rapid breathing and decreased appetite. Pathological examination of two randomly selected rats from each group showed destruction of alveolar structure accompanied by edema and hemorrhage, indicating successful ARDS modeling. The successfully modeled rats were then randomly divided into the LPS group, and XBJ low (XBJ-L), medium (XBJ-M), and high dose (XBJ-H) groups, with 10 rats in each group. Based on literature references and extensive preliminary experiments, the XBJ-L, XBJ-M, and XBJ-H groups received intraperitoneal injections of XBJ at doses of 4 mL/kg, 8 mL/kg, and 16 mL/kg, respectively.[8] The control and LPS groups received intraperitoneal injections of an equal volume of saline, twice daily for three consecutive days.

Tissue Sample Collection

The rats were anesthetized, and blood was collected from the abdominal aorta for ELISA detection. The rats were sacrificed and fixed in a supine position. Abdominal hair was removed, an incision was made in the abdomen, and the thoracic cavity was opened to collect lung tissue. The left lung tissue was used for dry/wet (D/W) ratio detection, and the upper lobe of the right lung was used for HE staining. The lower lobe was used for Western blot, qRT-PCR, and ELISA detection.

Dry/Wet (D/W) Ratio Assessment

The left lung tissue of the rats was blotted dry on the surface with clean filter paper, and the wet weight was recorded. The lung tissue was then placed in an oven at 80°C for 48 hours to obtain the dry weight. The D/W ratio was calculated to assess the water content of the lung tissue.

ELISA Detection of IL-17, IL-6, IL-1β, TNF-α, and MPO Levels in Lung Tissue

Samples and standards were pipetted into microplates pre-coated with antibodies and incubated at room temperature. A standard curve was prepared, and the optical density of each well was measured at 450 nm to analyze the levels of each factor.

HE Staining for Pathological Changes in Lung Tissue

The upper lobe of the right lung was flushed with cold phosphate-buffered saline, fixed in 10% neutral buffered formalin, embedded in paraffin, and sectioned. Sections were stained with HE and scored.[9] The degree of pathological changes was evaluated based on neutrophil infiltration in the alveolar or interstitial spaces, alveolar membrane thickening, and capillary congestion. The damage was assessed on a scale of 0–3, with 0 indicating no injury and 3 indicating severe injury. The cumulative scores were used for pathological damage assessment.

Immunohistochemical Detection of HIF-1α and ICAM-1 Expression in Lung Tissue

Tissue sections were prepared as described in the pathological section preparation steps. Paraffin was removed, and the sections were washed with PBS. The sections were treated with 1% hydrogen peroxide and 1% PBS/BSA, followed by incubation with HIF-1α and ICAM-1 antibodies diluted at 1:100. The sections were washed with PBS and then treated with secondary antibodies diluted at 1:500. After washing with PBS, the sections were treated with Tris-HCl buffer, DAB, and counterstained with hematoxylin, fixed with resin, and examined under an optical microscope. Random fields were selected under high magnification, and the area ratio of protein-positive staining was calculated.

Western Blot Detection of HIF-1α and ICAM-1 Protein Expression in Lung Tissue

Lung tissue was lysed on ice using RIPA lysis buffer. The total protein concentration was quantified using a BCA protein assay kit, and proteins were separated by 10% SDS-PAGE and transferred to PVDF membranes. The membranes were blocked with 5% non-fat milk to prevent non-specific binding. The membranes were then incubated with primary antibodies against HIF-1α and ICAM-1, followed by incubation with goat anti-rabbit or anti-mouse secondary antibodies.

Protein bands were visualized using an enhanced chemiluminescence kit, and quantitative analysis was performed using Image-Pro Plus software, with β-actin as the internal reference.

Statistical Analysis

The measurement data were expressed as mean ± standard deviation ($\bar{x} \pm s$). The experimental data were analyzed using SPSS 27.0 software, with P<0.05 considered statistically significant. One-way ANOVA was used for multiple group comparisons, followed by *snk-q* test for pairwise comparisons.

Results

Intersection Targets of XBJ and ARDS

The targets corresponding to "Carthami Flos", "Paeoniae Radix Rubra", "Angelicae Sinensis Radix", "Salviae Miltiorrhizae Radix et Rhizoma", and "Chuanxiong Rhizoma" in XBJ yielded 766 targets after deduplication. A total of 204 ARDS-related targets were collected through the GeneCards database. After constructing a Venn diagram, 46 intersecting targets between the compound-related targets and the disease-related targets were obtained, as shown in Figure 1.

Intersection Target Protein-Protein Interaction Network Diagram

The 46 intersection targets obtained were imported into the STRING database, with the species set to "Homo sapiens" and the confidence score set to 0.4. A protein-protein interaction (PPI) network was obtained, as shown in Figure 2. Due to the complexity and the large number of nodes in the protein-protein interaction network diagram, making it difficult to visually observe the relationships of the central nodes.Therefore, the obtained protein-protein interaction information was imported into Cytoscape software. Network Analyzer was used for further analysis of the PPI network, and core targets with a degree ≥ 30 were screened, resulting in 24 key targets, as shown in Figure 3. The node size corresponds to the degree value, with nodes becoming brighter as the degree increases. The deeper the red color in the figure, the higher the degree value.

GO Enrichment Analysis of Core Targets

The 26 key targets were imported into the DAVID platform, with the species set to human, for GO functional analysis. GO enrichment analysis is divided into three parts based on gene function: Cellular Components (CC), Molecular Function (MF), and Biological Processes (BP). Among them, MF has 22 entries, CC has 20 entries, and BP has 147 entries. The top 10 entries in each part based on Count values were selected for plotting. The entries with the highest Count values in MF, CC, and BP are heparin binding, extracellular space, and proteolysis, respectively, as shown in Figure 4.

KEGG Enrichment Analysis of Core Targets

KEGG enrichment analysis identified 53 related pathways. After excluding human disease-related terms,The top 20 pathways based on Count values were selected to draw a bubble chart. The intervention effects of XBJ on ARDS involve

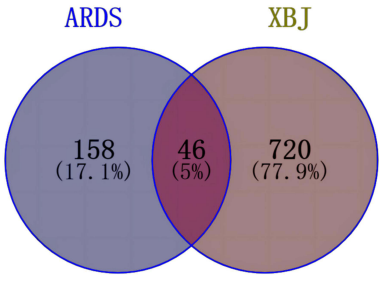

Figure 1 Venn Diagram of XBJ and ARDS related targets.

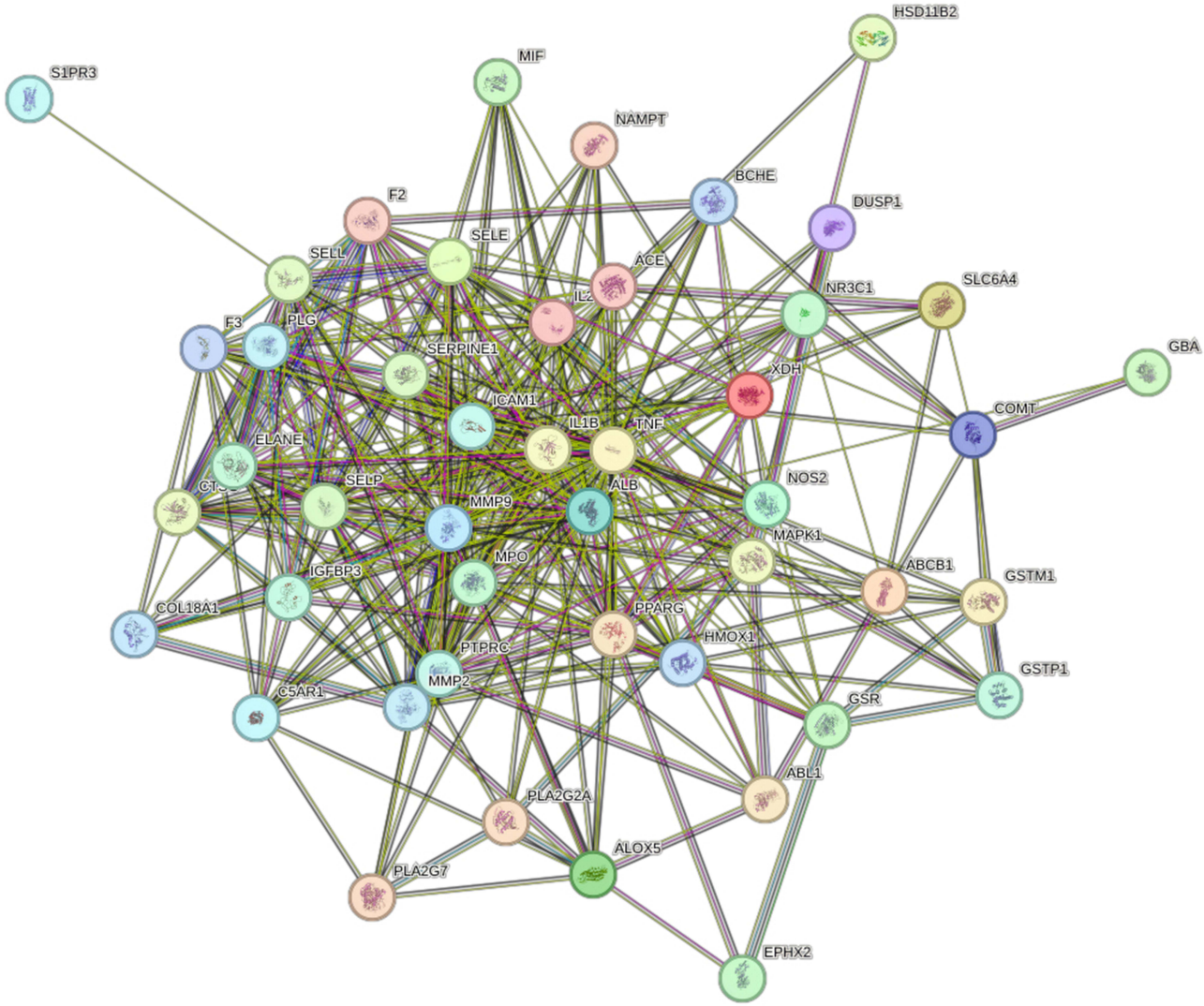

Figure 2 Protein interaction network diagram of 46 intersection targets.

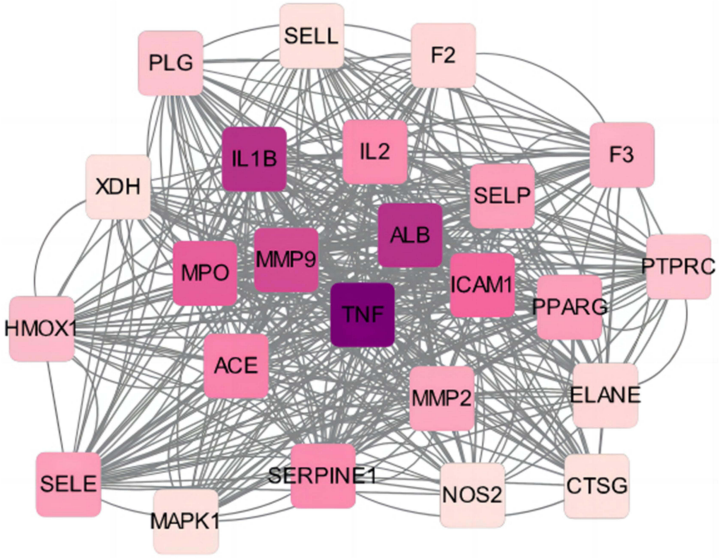

Figure 3 Plots of 24 core targets with a Degree≥30.

https://doi.org/10.2147/JIR.S507468

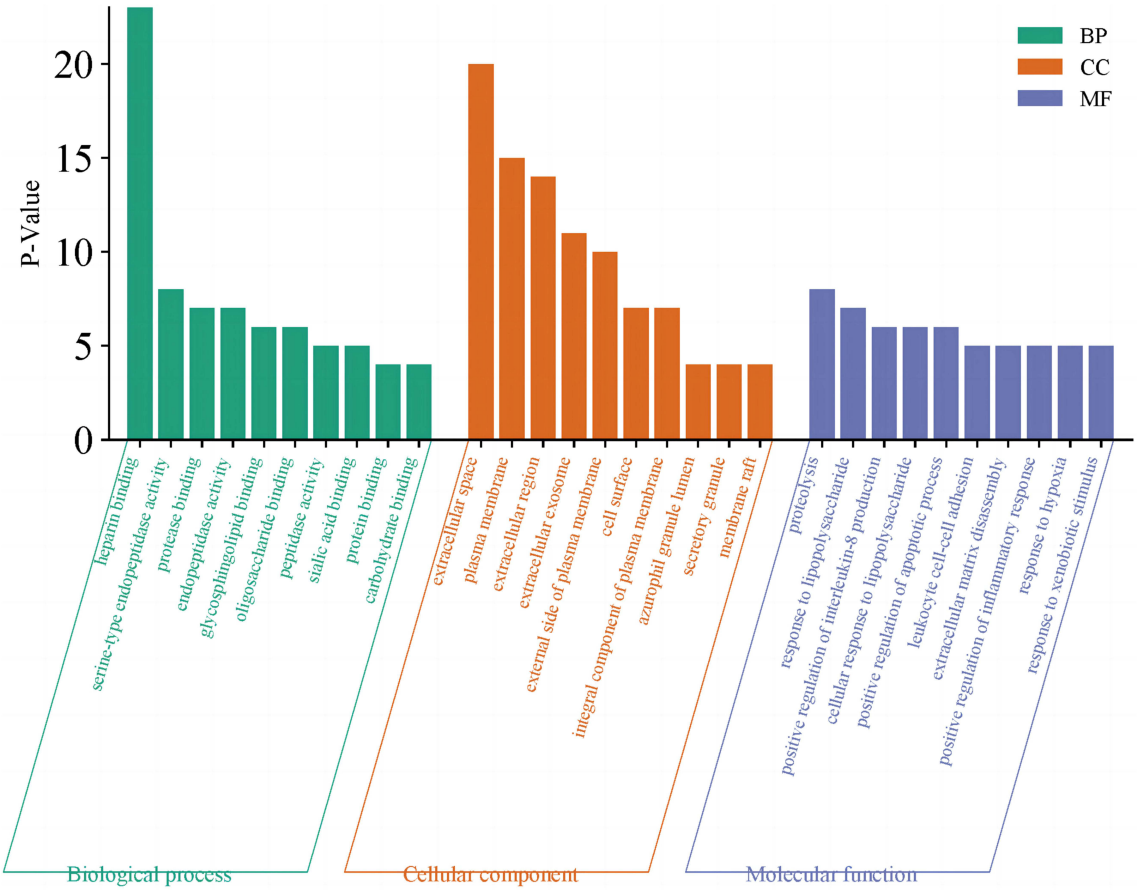

Figure 4 GO enrichment analysis diagram.

pathways such as T cell receptor signaling pathway, IL-17 signaling pathway, HIF-1 pathway, and TNF signaling pathway, as shown in Figure 5. The larger the bubble in the figure, the more genes are present in the pathway.

Effect of XBJ on D/W Ratio in Rats of Each Group

Compared with the control group, the D/W ratio in the LPS group was significantly increased (P<0.05). Compared with the LPS group, the D/W ratio in the XBJ-L, XBJ-M, and XBJ-H groups was significantly reduced, with the most significant reduction observed in the XBJ-H group. There were significant differences between the groups (P<0.05). See Table 1.

Effect of XBJ on Serum Levels of IL-17, IL-6, IL-1β, and TNF-α in Rats of Each Group

Compared with the control group, serum levels of IL-17, IL-6, IL-1β, and TNF-α in the LPS group were significantly increased (P<0.05). Compared with the LPS group, serum levels of IL-17, IL-6, IL-1β, and TNF-α in the XBJ-L, XBJ-M, and XBJ-H groups were significantly reduced, with the most significant reduction observed in the XBJ-H group. There were significant differences between the groups (P<0.05). See Table 2.

Effect of XBJ on MPO Levels in Lung Tissue of Rats in Each Group

Compared with the control group, MPO levels in lung tissue of the LPS group were significantly increased (P<0.05). Compared with the LPS group, MPO levels in lung tissue of the XBJ-L, XBJ-M, and XBJ-H groups were significantly reduced, with the most significant reduction observed in the XBJ-H group. There were significant differences between the groups (P<0.05). See Table 3.

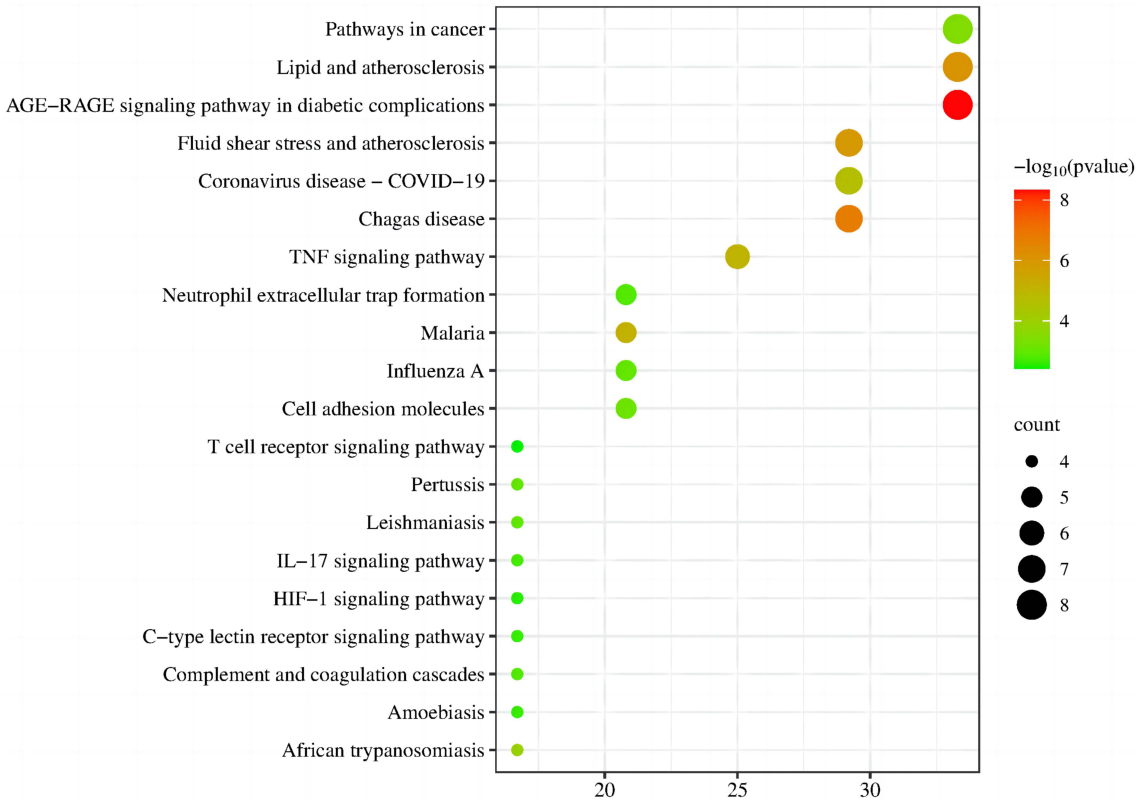

Figure 5 KEGG enrichment analysis diagram.

Effect of XBJ on Pathological Changes in Lung Tissue of Rats in Each Group

In the control group, the alveolar tissue structure of rats was intact with no significant pathological damage. In the LPS group, severe pathological damage was observed, with destroyed alveolar structure, hemorrhage, edema, and neutrophil infiltration. The pathological scores were significantly higher than those of the control group (P<0.05). After intervention with different doses of XBJ, the extent of alveolar structure damage was reduced, and the pathological scores were significantly lower than those of the LPS group (P<0.05), with the best improvement observed in the XBJ-H group. See Figure 6 and Table 4.

Table 1 Comparison of D/W Values of Rats in Each Group ($\bar{x} \pm s$, $n = 10$)

Groups	D/W
control	3.18±0.33
LPS	8.91±0.93[a]
XBJ-L	6.01±0.63[b]
XBJ-M	4.16±0.43[bc]
XBJ-H	3.22±0.34[bcd]

Notes: Compared with control group, [a]*P*<0.05; Compared with LPS group, [b]*P*<0.05; Compared with XBJ-L group, [c]*P*<0.05; Compared with XBJ-M group, [d]*P*<0.05.

https://doi.org/10.2147/JIR.S507468

Table 2 Comparison of IL-17, IL-6, IL-1β and TNF-α in Rats of Each Group ($\bar{x} \pm s$, $n = 10, pg/mL$)

Groups	IL-17	IL-6	IL-1β	TNF-α
Control	21.52±2.22	97.88±10.22	103.22±11.06	43.18±4.57
LPS	58.11±5.88[a]	288.01±29.11[a]	258.72±26.36[a]	143.24±14.85[a]
XBJ-L	43.85±4.51[b]	208.34±20.71[b]	192.42±19.42[b]	94.92±9.58[b]
XBJ-M	32.42±3.31[bc]	149.72±15.91[bc]	149.55±15.14[bc]	68.75±6.94[bc]
XBJ-H	23.42±2.44[bcd]	108.11±11.27[bcd]	111.28±12.06[bcd]	47.44±4.89[bcd]

Notes: Compared with control group, [a]*P*<0.05; Compared with LPS group, [b]*P*<0.05; Compared with XBJ-L group, [c]*P*<0.05; Compared with XBJ-M group, [d]*P*<0.05.

Table 3 Comparison of MPO Levels in Lung Tissues of Rats in Each Group ($\bar{x} \pm s$, $n = 10, U/g$)

Groups	MPO
control	1.85±0.19
LPS	5.24±0.56[a]
XBJ-L	3.81±0.40[b]
XBJ-M	2.82±0.31[bc]
XBJ-H	1.92±0.21[bcd]

Notes: Compared with control group, [a]*P*<0.05; Compared with LPS group, [b]*P*<0.05; Compared with XBJ-L group, [c]*P*<0.05; Compared with XBJ-M group, [d]*P*<0.05.

Effect of XBJ on HIF-1α and ICAM-1 Protein Expression in Lung Tissue of Rats in Each Group

Compared with the control group, the expression of HIF-1α and ICAM-1 proteins in the lung tissue of rats in the LPS group was significantly increased (P<0.05). Compared with the LPS group, the expression of HIF-1α and ICAM-1 proteins in the lung tissue of rats in the XBJ-L, XBJ-M, and XBJ-H groups was significantly decreased, with the most significant reduction observed in the XBJ-H group. There were significant differences between the groups (P<0.05). See Figure 7 and Table 5.

Discussion

ARDS is a disease characterized by severe inflammatory damage to alveolar cells and capillary membranes, leading to high permeability and infiltration of lung immune cells, and decreased oxygenation.[10] LPS-activated epithelial cells produce inflammatory factors that promote systemic/local responses and cell damage by signaling to endothelial cells.

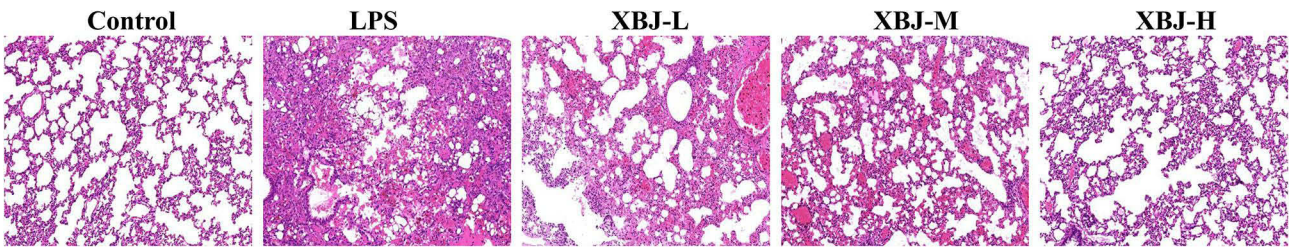

Figure 6 Lung histopathological changes (HE, ×200).

Table 4 Comparison of Pathological Scores of Rats in Each Group ($\bar{x} \pm s$, $n = 10$)

Groups	Pathological Scores
Control	0.15±0.02
LPS	12.25±1.34[a]
XBJ-L	7.81±0.82[b]
XBJ-M	5.06±0.53[bc]
XBJ-H	3.02±0.33[bcd]

Notes: Compared with control group, [a]$P<0.05$; Compared with LPS group, [b]$P<0.05$; Compared with XBJ-L group, [c]$P<0.05$; Compared with XBJ-M group, [d]$P<0.05$.

This can also lead to excessive activation of the immune system, altering physiological characteristics such as pulmonary vascular resistance, bronchoconstriction, and airway hyperresponsiveness, thereby resulting in ARDS.[6] The pathogenesis of ARDS is complex, involving organ inflammation, pulmonary immune homeostasis, systemic inflammation, and apoptosis, making it a refractory respiratory disease. Current prescription drugs such as statins, β-agonists, and corticosteroids have certain limitations,[11] necessitating the search for effective therapeutic drugs.

XBJ's main herbal components are Carthami Flos, Paeoniae Radix Rubra, Chuanxiong Rhizoma, Salviae Miltiorrhizae Radix et Rhizoma, and Angelicae Sinensis Radix. It is a traditional Chinese medicine based on the Blood Stasis Expelling Decoction and has various effects, including improving microcirculation, immune regulation, anti-inflammatory, and antioxidant properties. It has been used to treat severe pneumonia and sepsis.[12] However, the efficacy of XBJ in treating ARDS is not fully understood, and its mechanism of action remains unclear. Traditional methods are no longer sufficient to elucidate its mechanism due to the multi-target and multi-component nature of traditional Chinese medicine. This study used network pharmacology to explore the therapeutic mechanism of XBJ in treating ARDS. The TCMSP database was used to analyze the active ingredients in XBJ, and after constructing a Venn diagram, 46 potential targets were identified as playing important roles in the treatment of ARDS with XBJ. Using DisGENET and Genecard databases, protein interaction information was imported into Cytoscape software, identifying key molecules such as IL-17, TNF-α, and MPO, indicating that immune regulation and inflammatory response play significant roles in the development of ARDS, consistent with previous studies.[13,14] In vivo experiments showed that LPS-induced ARDS rats exhibited alveolar structural damage, increased D/W ratio, elevated serum levels of IL-17, IL-6, IL-1β, TNF-α, and lung tissue MPO levels, and higher pathological scores. However, these indicators were reversed after XBJ treatment, indicating that XBJ can improve immune function and inflammatory response in the treatment of ARDS.

GO and KEGG enrichment analyses indicate that the pathways most involved are those related to immune function and inflammatory response, further suggesting that XBJ's intervention in ARDS is achieved through immune regulation and inhibition of inflammation. The IL-17 signaling pathway, HIF-1 pathway, and TNF signaling pathway are associated with pulmonary inflammation and immune regulation. Previous studies have shown that hypoxia and pulmonary inflammation can promote ARDS. HIF-1, as a key regulator of hypoxia-ischemia, protects cells from hypoxia-

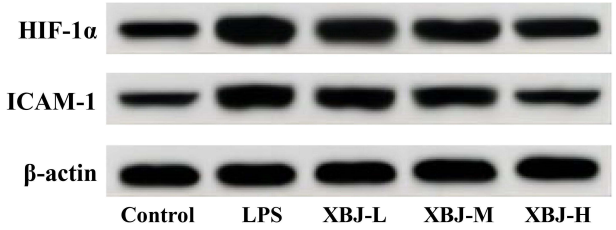

Figure 7 Expressions of HIF-1α and ICAM-1 proteins in lung tissue (Western blot).

https://doi.org/10.2147/JIR.S507468

Table 5 Comparison of HIF-1α and ICAM-1 Protein Expression in Lung Tissues of Each Group ($\bar{x} \pm s$, $n = 10$)

Groups	HIF-1α/β-Actin	ICAM-1/β-Actin
Control	0.39±0.40	0.21±0.03
LPS	1.52±0.17[a]	0.96±0.11[a]
XBJ-L	1.02±0.11[b]	0.65±0.07[b]
XBJ-M	0.72±0.08[bc]	0.41±0.05[bc]
XBJ-H	0.44±0.05[bcd]	0.28±0.03[bcd]

Notes: Compared with control group, [a]*P*<0.05; Compared with LPS group, [b]*P*<0.05; Compared with XBJ-L group, [c]*P*<0.05; Compared with XBJ-M group, [d]*P*<0.05.

ischemia-mediated injury.[15] Inflammation and hypoxia can stimulate and activate HIF-1α and related pathways, inducing human lung epithelial cell damage and participating in ARDS development. Suresh et al[16] found that myo-inositol can reduce ARDS-induced pulmonary fibrosis by inhibiting HIF-1 expression. TNF-α, the most studied cytokine in the TNF family, can induce inflammatory responses. Inhibiting this pathway can effectively treat ARDS.[17,18] ICAM-1 is a cell surface glycoprotein that plays an important role in neutrophil infiltration into the lungs and serves as a biomarker for assessing the severity and outcomes of ARDS. Studies have shown that inhibiting ICAM-1 helps improve LPS-induced ARDS in rats.[19,20] Our in vivo experimental results also confirmed that HIF-1α and ICAM-1 protein expressions were upregulated in the lung tissue of ARDS rats. After XBJ intervention, the expressions of HIF-1α and ICAM-1 proteins in the lung tissue decreased, suggesting that XBJ's treatment of ARDS is related to multiple pathways, including the IL-17 signaling pathway, HIF-1 pathway, and TNF signaling pathway.

Conclusion

In conclusion, the network pharmacology-based analysis of XBJ's potential molecular mechanisms in ARDS, including the IL-17 signaling pathway, HIF-1 pathway, and TNF signaling pathway, plays a key role in alleviating pulmonary inflammation and slowing the progression of ARDS. The integration of network pharmacology and animal experiments not only provides an efficient tool for elucidating the mechanisms of ARDS and developing new drugs, but also promotes clinical translation through multi-dimensional validation—from molecular targets to overall therapeutic effects. Especially in the current context where effective treatments are lacking, this research model holds significant value for improving patient prognosis and reducing healthcare burdens. However, given the complexity of ARDS-related molecules and signaling pathways, further studies will focus on these aspects for continued exploration.

Data Sharing Statement

All relevant data are within the paper.

Ethics Approval

All animal experiments complied with the ARRIVE guidelines and performed in accordance with the National Institutes of Health Guide for the Care and Use of Laboratory Animals. The study was approved by Ganzhou People's Hospital ethics review board (No.GZSRMYY2024110021) and with the 1964 helsinki Declaration.

Consent for Publication

All authors give consent for publication.

Funding

Jiangxi Provincial Health Commission Plan Project (202311957).

Disclosure

All authors declare no conflicts of interest in this work.

References

1. Dupuis J, Sirois MG, Rhéaume E. et al. Colchicine reduces lung injury in experimental acute respiratory distress syndrome. *PLoS One*. 2020;15 (12):e0242318. doi:10.1371/journal.pone.0242318
2. Wang X, Liu F, Xu M, Wu L. Penehyclidine hydrochloride alleviates lipopolysaccharide-induced acute respiratory distress syndrome in cells via regulating autophagy-related pathway. *Mol Med Rep*. 2021;23(2):1.
3. Meyer NJ, Gattinoni L, Calfee CS. Acute respiratory distress syndrome. *Lancet*. 2021;398(10300):622–637. doi:10.1016/S0140-6736(21)00439-6
4. Li C, Wang P, Zhang L, et al. Efficacy and safety of Xuebijing injection (a Chinese patent) for sepsis: a meta-analysis of randomized controlled trials. *J Ethnopharmacol*. 2018;224:512–521. doi:10.1016/j.jep.2018.05.043
5. Dong R, Huang R, Shi X, Xu Z, Mang J. Exploration of the mechanism of luteolin against ischemic stroke based on network pharmacology, molecular docking and experimental verification. *Bioengineered*. 2021;12(2):12274–12293. doi:10.1080/21655979.2021.2006966
6. Simões JS, Rodrigues RF, Zavan B, Emídio RMP, Soncini R, Boralli VB. Endotoxin-Induced Sepsis on Ceftriaxone-Treated Rats' Ventilatory Mechanics and Pharmacokinetics. *Antibiotics*. 2024;13(1):83. doi:10.3390/antibiotics13010083
7. Tirunavalli SK, Gourishetti K, Kotipalli RSS, et al. Dehydrozingerone ameliorates Lipopolysaccharide induced acute respiratory distress syndrome by inhibiting cytokine storm, oxidative stress via modulating the MAPK/NF-κB pathway. *Phytomedicine*. 2021;92:153729. doi:10.1016/j.phymed.2021.153729
8. Lv J, Guo X, Zhao H, Zhou G, An Y. Xuebijing Administration Alleviates Pulmonary Endothelial Inflammation and Coagulation Dysregulation in the Early Phase of Sepsis in Rats. *J Clin Med*. 2022;11(22):6696. doi:10.3390/jcm11226696
9. Xu H-R, Yang Q, Xiang S-Y, et al. Rosuvastatin Enhances Alveolar Fluid Clearance in Lipopolysaccharide-Induced Acute Lung Injury by Activating the Expression of Sodium Channel and Na,K-ATPase via the PI3K/AKT/Nedd4-2 Pathway. *J Inflamm Res*. 2021;14:1537–1549. doi:10.2147/JIR.S299267
10. Silva PL, Pelosi P, Rocco PRM. Personalized pharmacological therapy for ARDS: a light at the end of the tunnel. *Expert Opin Investig Drugs*. 2020;29(1):49–61.
11. Ding Q, Zhu W, Diao Y, et al. Elucidation of the Mechanism of Action of Ginseng Against Acute Lung Injury/Acute Respiratory Distress Syndrome by a Network Pharmacology-Based Strategy. *Front Pharmacol*. 2020;11:611794. doi:10.3389/fphar.2020.611794
12. Tianyu Z, Liying G. Identifying the molecular targets and mechanisms of xuebijing injection for the treatment of COVID-19 via network pharmacology and molecular docking. *Bioengineered*. 2021;12(1):2274–2287. doi:10.1080/21655979.2021.1933301
13. Zhang Y, Wang J, Liu Y-M, Yang H, Wu G-J, He X-H. Analysis of the Efficacy and Mechanism of Action of Xuebijing Injection on ARDS Using Meta-Analysis and Network Pharmacology. *Biomed Res Int*. 2021;2021(1):8824059. doi:10.1155/2021/8824059
14. Shang T, Zhang Z-S, Wang X-T, et al. Xuebijing injection inhibited neutrophil extracellular traps to reverse lung injury in sepsis mice via reducing Gasdermin D. *Front Pharmacol*. 2022;13:1054176. doi:10.3389/fphar.2022.1054176
15. Zhang Z, Yao L, Yang J, Wang Z, Du G. PI3K/Akt and HIF-1 signaling pathway in hypoxia-ischemia (Review). *Mol Med Rep*. 2018;18 (4):3547–3554. doi:10.3892/mmr.2018.9375
16. Suresh MV, Yalamanchili G, Rao TC, et al. Hypoxia-inducible factor (HIF)-1α-induced regulation of lung injury in pulmonary aspiration is mediated through NF-kB. *FASEB Bioadv*. 2022;4(5):309–328. doi:10.1096/fba.2021-00132
17. Qiao Q, Liu X, Yang T, et al. Nanomedicine for acute respiratory distress syndrome: the latest application, targeting strategy, and rational design. *Acta Pharm Sin B*. 2021;11(10):3060–3091. doi:10.1016/j.apsb.2021.04.023
18. Cui Y, Wang X, Lin F, et al. MiR-29a-3p Improves Acute Lung Injury by Reducing Alveolar Epithelial Cell PANoptosis. *Aging Dis*. 2022;13 (3):899–909. doi:10.14336/AD.2021.1023
19. He B, Geng S, Zhou W, et al. MMI-0100 ameliorates lung inflammation in a mouse model of acute respiratory distress syndrome by reducing endothelial expression of ICAM-1. *Drug Des Devel Ther*. 2018;12:4253–4260. doi:10.2147/DDDT.S188095
20. Yao M-Y, Zhang W-H, Ma W-T, Liu Q-H, Xing L-H, Zhao G-F. Long non-coding RNA MALAT1 exacerbates acute respiratory distress syndrome by upregulating ICAM-1 expression via microRNA-150-5p downregulation. *Aging*. 2020;12(8):6570–6585. doi:10.18632/aging.102953